Journal of Natural Gas Science and Engineering xxx (2015) 1–14

Contents lists available at ScienceDirect

Journal of Natural Gas Science and Engineering

journal homepage: www.elsevier.com/locate/jngse

A sequential model of shale gas transport under the influence of fully coupled multiple processes

Yan Peng [a], Jishan Liu [a, b, *], Zhejun Pan [c], Luke D. Connell [c]

[a] School of Mechanical and Chemical Engineering, The University of Western Australia, 35 Stirling Highway, WA 6009, Australia
[b] State Key Laboratory of Geomechanics and Geotechnical Engineering, Institute of Rock and Soil Mechanics, Chinese Academy of Sciences, Hubei 430071, China
[c] CSIRO Energy Flagship, Private Bag 10, Clayton South 3169, Australia

ARTICLE INFO

Article history:
Received 29 June 2015
Received in revised form
16 September 2015
Accepted 16 September 2015
Available online xxx

Keywords:
Numerical simulation
Shale gas flow
Geomechanical effect
Apparent permeability

ABSTRACT

Shales have complex microscopic pore structures which significantly affect shale gas production. Effects of microscopic pore structure on flow regimes have been widely investigated. The pressure dependent permeability in shales has been also observed in laboratory and it may cause more significant variation in apparent permeability than flow regimes does. Therefore, numerical models combining flow regimes and pressure dependent permeability are required to describe the gas flow behaviour in shales. In this study, based on literature experimental observations, a numerical simulation model for shale gas transport was built. The model includes the main gas flow characteristics in shale: (1) sequential flow process of different flow regimes for different pores; (2) variation of apparent permeability resulted from both flow regimes and stress variation in shale; (3) permeability change with respect to strain. Nine sets of literature experimental data were used to verify this numerical simulation model, which was shown to be able to accurately describe the data. Using this numerical simulation model, shale gas flow behaviour was analysed and the following conclusions were found: (1) the effect of shale deformation on gas production is significant. Compared with other factors, it is a considerably important factor controlling the apparent permeability evolution during shale reservoir depletion; (2) natural fracture plays a significant role in gas transport inside reservoirs. Although its porosity is much less than those of other pores, it could obviously enhance shale gas recovery rate because of its higher permeability; (3) natural fracture permeability, natural fracture porosity, inorganic pores permeability and Young's modulus have positive correlations with shale gas recovery rate. However, the percentage of adsorbed gas has a negative correlation with shale gas recovery rate.

1. Introduction

The production behaviour of shale gas may have an inherent link with its diversity of minerals and the complexity in microscopic structure. Shales normally contain quartz, clays, carbonates, and organic material (e.g. kerogen) (Wang and Reed, 2009; Sondergeld et al., 2010). They are also consisted of pores with a wide range of sizes (Nelson, 2009; Loucks et al., 2012). Characteristics of shales make the gas storage and flow in shale different from other porous media. For instance, majority of methane stores as adsorbed phase in coals, while both free gas and adsorbed gas have considerable amount in shales (Curtis, 2002; Olsen et al., 2003). In laboratory, a huge difference in methane release behaviours between shales and coals was observed (Javadpour et al., 2007).

In shale-gas systems, the microscopic pore structure contains matrix-related pores and natural fractures. The matrix-related pores are composed of nanometre-to micrometre-size pores. The natural fracture connects to hydraulic fractures and its network plays an important role in shale gas production (Gale et al., 2007). The unique microscopic structure of shales affects gas production in two main aspects. First, the process of gas release from shales experiences several flow regimes due to its complex network of flow path in shales. The flow regimes for different size pores could be significantly different. To classify them, the Knudsen number, the ratio of the mean-free-path of gas to the pore diameter is used to distinguish these regimes from the free-molecule flow to the

* Corresponding author. School of Mechanical and Chemical Engineering, The University of Western Australia, 35 Stirling Highway, WA 6009, Australia.
E-mail address: jishan.liu@uwa.edu.au (J. Liu).

http://dx.doi.org/10.1016/j.jngse.2015.09.031
1875-5100/

continuum flow (Roy et al., 2003). Secondly, pores in shales would experience complex geomechanical deformations during shale gas depletion. The geomechanical deformations significantly affect apertures of flow paths which determine permeability. Therefore, an effective numerical simulation model should contain all these effects of microscopic structure on shale gas production.

To involve deviation of gas flow regimes, many numerical simulation models for gas transport in shales have been proposed and Knudsen number is widely used to differentiate the flow regions in shales (e.g., Civan et al., 2011; Javadpour, 2009; Ye et al., 2015). Non-Darcy equations for gas flow, which include Knudsen diffusion and slip flow, have also been proposed and studied (e.g., Guo et al., 2015; Javadpour, 2009; Moghadam and Chalaturnyk, 2014). However, flows in different regions are not only different but also interacting with each other. Early work considering interactions between different flow paths is dual-porosity model for porous media proposed by Warren and Root (1963). Such dual-porosity approach has been adopted to describe flow in shales (Carlson and Mercer, 1991). Nevertheless, dual-porosity models treat the fluid in matrix as a source of the flow in fractures and ignore fluid flow in matrix. Other work tried to account for flows in different flow paths. For instance, multi-continua at the naturally fractured reservoirs was developed and applied (Bear and Bachmat, 1990). For shale reservoirs where gas flows in both matrix pores and fracture system, a multi-scale model combining dual-porosity concept and multi-continua theory for gas transport in shales has been proposed (Kang et al., 2011; Akkutlu and Fathi, 2012). The advantage of these models is that interactions between different flow paths can be mathematically described. Other method to include interactions between different flow regions is the multiple interacting continua (MINC) method (Pruess, 1985). In the MINC method, each matrix block is subdivided into several nested "sub-cells" and interactions in matrix blocks are defined by connecting factors between these sub-cells. Rubin (2010) used this method to investigate shale gas production. This method was improved by determining inter-cell connecting factors (Ding et al., 2014). To account for effect of microscopic structure on gas flow, the apparent permeability (k_{app}) is applied in all studies mentioned above. However, they only focused on the correlation coefficient (k_g) between k_{app} and intrinsic permeability (k_∞), which is assumed to be constant. Nevertheless, it is not appropriate to assume constant intrinsic permeability because the intrinsic permeability significantly changes during shale gas depletion.

The intrinsic permeability has a close relationship with diameter of pores and porosity of rocks (e.g., Nelson, 2009; Cho et al., 2013). During shale gas depletion, the geomechanical deformation of shales can dramatically affect porosity so the intrinsic permeability is often observed as pressure dependent. The pressure and field production data demonstrated evidence of pressure dependent permeability in Horn River and Haynesville shales (Vera and Ehlig-Economides, 2013). Laboratory measurements also showed that intrinsic permeability decreases with effective stress (Dong et al., 2010; Tinni et al., 2012; Heller et al., 2014; Wang et al., 2014; Ghanizadeh et al., 2015). Comparisons between Klinkenberg effect and effective stress effect on permeability of shales were investigated in laboratory as well. When pore pressure exceeds 500 psi (around 3.5 MPa), the Klinkenberg effect would not significantly affect permeability (Wang and Reed, 2009). Effective stress, ranging from 0 MPa to 100 MPa, always significantly affects shale permeability (Dong et al., 2010; Wang et al., 2014). To account for the large change in intrinsic permeability during gas production, numerical simulations require an intrinsic permeability model.

Currently, great efforts have been made to model intrinsic permeability of porous media. It has been pointed out that the change of intrinsic permeability has an exponential relationship with effective stress (Rutqvist et al., 2002) or the strain of porous media (Minkoff et al., 2003). Mechanical conditions in the field are usually assumed as uniaxial strain and constant overburden (e.g., Shi and Durucan, 2005). Under this condition, intrinsic permeability has a relationship with pore pressure (Raghavan and Chin, 2002). In order to incorporate the effect of methane adsorption into intrinsic permeability models for coal reservoirs, many models with stress-based and strain-based forms have been proposed according to the field conditions (e.g. Gray, 1987; Palmer and Mansoori, 1996; Shi and Durucan, 2005). To overcome their limits resulted from assumption of mechanical conditions, an improved permeability model was proposed by Palmer et al. (2007) and a model derived from poroelastic theory was proposed by Zhang et al. (2008). These models were valid for a single porosity medium. Shale contains several pore structures and is not a single porosity medium. Therefore, it is not applicable to use these models to describe the intrinsic permeability for shales. In general, intrinsic permeability of matrix system is several orders of magnitude lower than that of fracture system in fractured media such as coals and shales (Han et al., 2010; Ghanizadeh et al., 2015). In this case, mass transfer between fractures and matrix is a dynamic process. The importance of these interactions for intrinsic permeability has been illustrated for coal reservoirs (Harpalani and Chen, 1997; Liu and Rutqvist, 2010; Liu et al., 2011; Peng et al., 2014a). To incorporate this impact on intrinsic permeability, several numerical simulation models for coal have been proposed (Wu et al., 2010; Peng et al., 2014b).

Gas flow regimes in shales significantly affect mass transfer thus it affects intrinsic permeability change and in return, a change in intrinsic permeability will also significantly influence gas flow behaviours in different flow regions. Traditional multi-scale models for shale gas flow only consider complex gas flow regimes. Intrinsic permeability models rarely consider characteristics of gas flow in shales. To fully represent gas flow in shales, considering the mutual influence of flow regimes and intrinsic permeability would improve gas production prediction. In this paper, a multi-scale numerical simulation model with mutual influence was proposed. To achieve this, several gas flow equations of different flow regimes as well as intrinsic permeability model were developed and coupled with a deformation equation controlling deformation of shale reservoir included. Using experimental data, the intrinsic permeability model was first verified. Then, behaviours of gas flow and apparent permeability in shales during shale gas production were studied. Finally, impacts of several key factors on shale gas production were analysed.

2. Conceptual model

2.1. Multi-scale model

Due to the diversity in minerals and wide range of pore sizes in shales, the gas flow in shales is a combination of different controlling processes as shown in Fig. 1. Once gas production commences, flow behaviours in pores with different sizes occur differently: (a) the gas initially adsorbed on the surfaces of kerogen (or clay minerals) pores desorbs almost immediately; (b) gas diffuses from organic pores into inorganic pores; (c) gas in inorganic pores flows into natural fractures; (d) gas in natural fractures flows into hydraulic fractures then to production well. According to the Knudsen number, these gas flow behaviours in reservoir can be described in several flow regimes: (a) gas flow regime in kerogen is diffusion; (b) gas flow regime in inorganic pores networks is slip flow; and (c) gas flow regime in natural fractures is Darcy flow (Javadpour et al., 2007).

In shales, these flow regimes sequentially dominate shale gas

Please cite this article in press as: Peng, Y., et al., A sequential model of shale gas transport under the influence of fully coupled multiple processes, Journal of Natural Gas Science and Engineering (2015), http://dx.doi.org/10.1016/j.jngse.2015.09.031

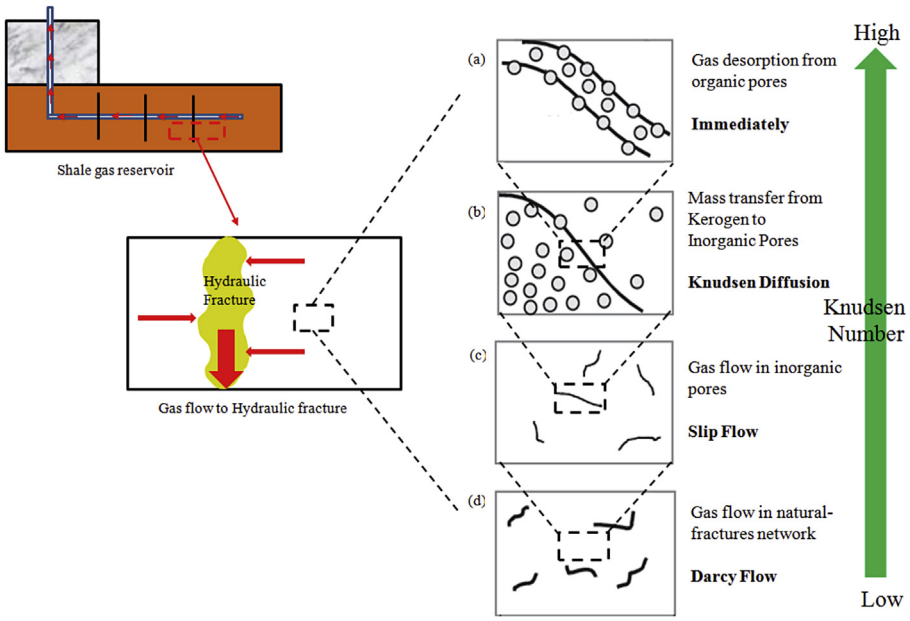

Fig. 1. Gas flow pattern in shales (modified from Javadpour et al., 2007).

production, which is different from gas flow in other porous media. Fig. 2 shows the comparison in experimental observation of gas release between coals and shales (Javadpour et al., 2007). The gas flow in coal has one dominated flow regimes but the gas flow in shale experiences different dominated flow regimes (shown as A, B, C and D in Fig. 2(b)). These curves named as A, B, C and D represent probability densities of corresponding flow regimes. Time spans of these curves are different. It indicates that these flow regimes occur at different time and sequentially dominate in the process of shale gas release. Therefore, the single-porosity model representing only one dominated flow regime is not proper therefore the multi-scale model is required in the numerical simulation of shale gas production.

The structure of multi-scale model with three modules in this study is shown in Fig. 3. The first module represents desorption and diffusion in kerogen and it covers processes (a) and (b) shown in Fig. 1. These two processes can be represented together because desorption in kerogen can be considered instantaneous and it is a function of pressure in kerogen. In this study, desorbed gas is treated as a source of diffusion in kerogen. The second module represents slip flow in inorganic pores and it covers process (c) shown in Fig. 1. The third module represents Darcy flow in natural fractures and it covers process (d) shown in Fig. 1. These modules are linked by mass transfer terms.

2.2. Effects of microscopic structure on apparent permeability

For multi-scale models, different flow regimes have different mathematical forms for flow velocity. In order to use the Darcy-type equation to present other non-Darcy flows, the common method is to introduce a variable, the apparent permeability (k_{app}), into corresponding velocity expressions. The apparent permeability is the result of intrinsic permeability (k_∞) and correlation coefficient (k_g):

$$k_{app} = k_\infty k_g \tag{1}$$

The correlation coefficient depends on flow regimes and the intrinsic permeability is determined by apertures of pores. With gas depletion, gas pressure in shales decreases, leading to changes in pore size (Chen et al., 2015) and thus intrinsic permeability

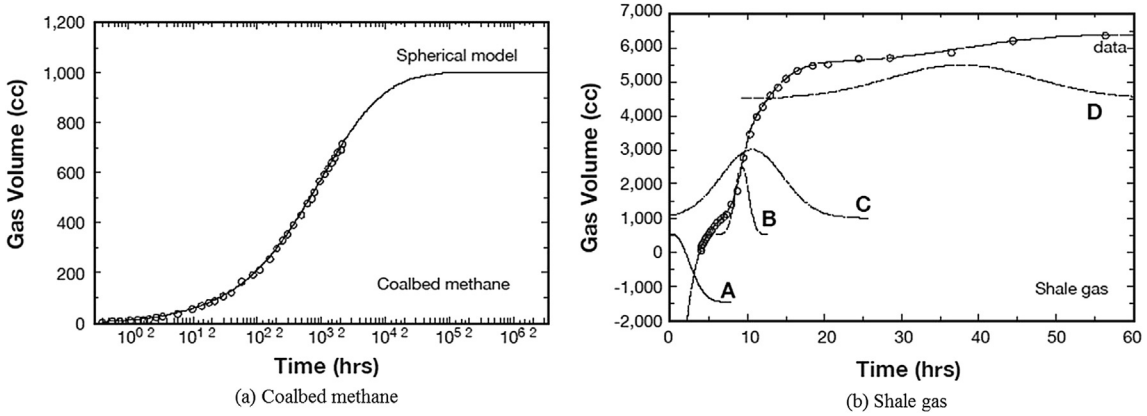

Fig. 2. Comparison of gas release between coalbed methane and shale gas (from Javadpour et al., 2007).

Please cite this article in press as: Peng, Y., et al., A sequential model of shale gas transport under the influence of fully coupled multiple processes, Journal of Natural Gas Science and Engineering (2015), http://dx.doi.org/10.1016/j.jngse.2015.09.031

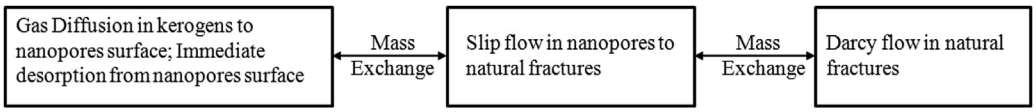

Fig. 3. Illustration of Structure of Multi-Scale Simulation Model in this Study.

changes. Characteristics of pore deformations in shales can be illustrated by a two-step process shown in Fig. 4: (1) Global strain as shown in Fig. 4(b). When gas is produced from reservoirs, the shale as a whole will deform and pores will shrink because of the increase in effective stress; (2) Local strain as shown in Fig. 4(c). It is resulted from interactions between different pore systems. Flow capacities of different pore systems (organic pores in kerogen, inorganic pores and natural fractures) are quite different. This may cause different dynamic changes in pressures of these pore systems. The pressure difference between them can induce further deformations of these pores. If the pressure in natural fracture is less than the pressures in inorganic pores and organic pores, the matrix block containing inorganic pores and kerogen would swell and the openings of the natural fractures would further decease. Furthermore, gas-rock interactions are correspondingly different with different minerals and this difference also induces different deformations among different pore systems. For kerogen and clay minerals, gas adsorbs to them, which leads to adsorption-induced strain (Chen et al., 2015). For other minerals, the adsorption-induced strain is negligible.

Multiple flow regimes coexist in shales and their intrinsic permeability changes differently. To properly cover all effects of microscopic structure on shale gas production, numerical simulation model should include gas flow equations to represent different gas flow regimes, a deformation equation to represent geomechanical behaviour of shale sediments, and, an equation to represent adsorption-induced strain as well as proper apparent permeability models. In the following section, the fully coupled simulation model for shale gas transport was proposed and introduced from these aspects.

3. Formulation of the conceptual model

3.1. Governing equation of the mechanical process

For dual porosity media, the mechanical process is described by the equation of motion for the mixture of matrix and fractures. On the basis of poroelasticity and by making an analogy between thermal contraction and adsorption-induced swelling, the equation of motion for dual porosity media is (Wu et al., 2010):

$$Gu_{i,kk} + \frac{G}{1-2\nu}u_{k,ki} - \alpha_f p_{f,i} - \alpha_m p_{m,i} - \varepsilon_{s,i} + f_i = 0 \tag{2}$$

where $G = E/2(1+\nu)$,$K = E/3(1-2\nu)$, α_f and α_m are Biot's coefficients for dual porosity media, G is the shear modulus of rock, E is the Young's modulus of rock, ν is Poisson's ratio of rock, K is the bulk modulus of shales, p_f is the natural fracture pressure, p_m is the matrix pressure, ε_s is the gas sorption-induced strain, and f is the body force of shales, u is the displacement.

Shale is a multi-porosity medium which contains natural fractures, inorganic pores, kerogen pores. Each component contributes to the mechanical deformation of shales. Similar to the deformation equation for dual porosity media (Eq. (2)), the deformation equation for the shale is:

$$Gu_{i,kk} + \frac{G}{1-2\nu}u_{k,ki} - \alpha_f p_{f,i} - \alpha_{na} p_{na,i} - \alpha_{ke} p_{ke,i} - \varepsilon_{s,i}(p_{ke}) + f_i = 0 \tag{3}$$

where α_f, α_{na} and α_{ke} are Biot's coefficients for shales, inorganic pores and kerogen, respectively, p_f is the natural fracture pressure, p_{na} is the inorganic pores pressure, p_{ke} is the kerogen pressure, ε_s is the gas sorption-induced strain of kerogen and it is a function of p_{ke} because that the adsorption only occurs in kerogen in shales.

From this equation, the shale volumetric strain (ε_v) can be calculated:

$$\varepsilon_v = \varepsilon_{11} + \varepsilon_{22} + \varepsilon_{33} \tag{4}$$

where ε_{11}, ε_{22} and ε_{33} are three principal strains.

In this study, the sorption-induced strain for kerogen can be assumed to be Langmuir equation like as demonstrated by the experimental measurement of methane adsorption induced shale swelling (Chen et al., 2015):

$$\varepsilon_s = \frac{\varepsilon_L p_{ke}}{P_L + p_{ke}} \tag{5}$$

where ε_L is the Langmuir strain constant, P_L is Langmuir pressure constant for strain.

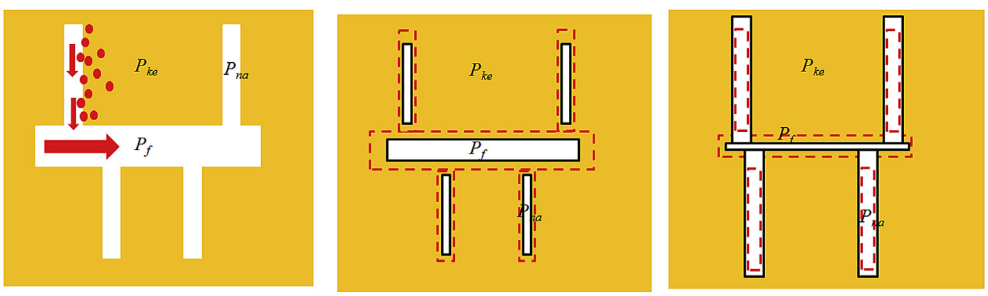

(a) Initial Apertures of Pores in Shales

(b) Deformation of Pores Caused by Global Strain

(c) Deformation of Pore Caused by Local Strain

Fig. 4. Illustration of Deformation Behaviour of Pores in Shales (P_{ke} is gas pressure in kerogen bulks; P_{na} is gas pressure in nanopores; P_f is gas pressure in natural fractures; Dashed rectangle represents original configuration of pores; Solid rectangle represents configuration of pores after deformation).

Please cite this article in press as: Peng, Y., et al., A sequential model of shale gas transport under the influence of fully coupled multiple processes, Journal of Natural Gas Science and Engineering (2015), http://dx.doi.org/10.1016/j.jngse.2015.09.031

3.2. Governing equations of gas flow in natural fracture networks

The gas flow regime in natural fracture networks is Darcy flow and the gas in natural fractures is in free gas phase form. The gas mass can be thus expressed by:

$$m = \phi_f \rho \tag{6}$$

where ρ is the free-phase gas density at fracture pressure, and ϕ_f is fracture porosity.

Applying the mass conservation law and Darcy velocity to the gas phase, it gives:

$$\frac{\partial m}{\partial t} + \nabla \cdot \left(-\frac{k_f}{\mu} \rho \nabla p_f \right) = Q_{f-na} \tag{7}$$

Substituting Eq. (6) into Eq. (7), the final governing equation of gas flow in the natural fracture networks is obtained:

$$p_f \frac{\partial \phi_f}{\partial t} + \phi_f \frac{\partial p_f}{\partial t} + \left(-\frac{k_f}{\mu} p_f \nabla p_f \right) = Q_{f-na} \tag{8}$$

where k_f is the natural fracture permeability, μ is viscosity and $Q_{f\text{-}na}$ is the mass transport rate between natural fractures and inorganic pores networks.

3.3. Governing equations of gas flow in inorganic pores

The gas flow regime in inorganic pores is Slip flow and the gas in inorganic pores networks is free gas phase form. The gas mass can be thus expressed by:

$$m = \phi_{na} \rho \tag{9}$$

where ρ is the free-phase gas density at inorganic pore pressure, and ϕ_{na} is inorganic pores porosity.

Applying the mass conservation law, it gives:

$$\frac{\partial m}{\partial t} + \nabla \cdot \left(\rho \mathbf{u}_{slip} \right) = -Q_{f-na} + Q_{na-ke} \tag{10}$$

The velocity of Slip flow for shale gas is (Javadpour, 2009):

$$\mathbf{u}_{slip} = -F \frac{k_{na}}{\mu} \nabla p_{na} \tag{11}$$

$$F = 1 + \left(\frac{8\pi RT}{M} \right)^{0.5} \frac{\mu}{p_{na} r_{na}} \left(\frac{2}{\alpha} - 1 \right) \tag{12}$$

where F is the correlation coefficient, k_{na} is the intrinsic permeability of inorganic pores. R is the gas constant, T is the temperature, M is the molecular mass of the gas, r_{na} is the radius of inorganic pores, α is the tangential momentum accommodation coefficient and its value varies in a range from 0 to 1.

Substituting Eqs. (11) and (12) into Eq. (10), it obtains the governing equation of gas flow in the inorganic pores networks:

$$\phi_{na} \frac{\partial p_{na}}{\partial t} + \nabla \left(-F \frac{k_{na}}{\mu} p_{na} \nabla p_{na} \right) = -Q_{f-na} + Q_{na-ke} \tag{13}$$

where $Q_{na\text{-}ke}$ is the mass transport rate between inorganic pores networks and kerogen.

3.4. Gas flow in kerogen

The gas in kerogen exists in both free gas phase and adsorbed phase forms. The gas mass can be thus expressed by:

$$m = \phi_{ke} \rho + \rho_{ad} \tag{14}$$

Assuming the density of adsorbed gas is subject to the Langmuir isotherm:

$$\rho_{ad} = \rho_{ga} \rho_s \frac{V_L p_{ke}}{P_L + p_{ke}} \tag{15}$$

The kerogen is one component of matrix blocks. It is assumed that kerogen connect to inorganic pores. In this case, the gas in kerogen serves as a mass source of the gas flow in the inorganic pores system. The spatial gas transport in kerogen is negligible because kerogen is discretely distributed in shales. Therefore, the gas mass change in kerogen equals to gas mass transfer between kerogen and inorganic pores. Applying the mass conservation law, it gives:

$$\frac{\partial m}{\partial t} = -Q_{na-ke} \tag{16}$$

Substituting Eqs. (14) and (15) into Eq. (16), the governing equation of gas flow in the kerogen can be obtained:

$$\phi_{ke} \frac{\partial \rho}{\partial t} + \rho_{ga} \rho_s \frac{V_L P_L}{(P_L + p_{ke})^2} \frac{\partial p_{ke}}{\partial t} = -Q_{na-ke} \tag{17}$$

where ρ is the free-phase gas density at kerogen pressure, ρ_{ad} is the density of adsorbed-phase gas, ϕ_{ke} is inorganic pores porosity, and V_L and P_L are Langmuir constants, ρ_s is the shale density and ρ_{ga} is gas density at atmosphere pressure.

3.5. Governing equation of mass transfer

The transport scheme is assumed as a pseudo steady-state so the rate of mass transfer is proportional to the pressure difference between these two systems (Ranjbar and Hassanzadeh, 2011). For the Darcy flow, the general mass transfer equation is:

$$q = \frac{\sigma k}{\mu} \rho \left(p_m - p_f \right) \tag{18}$$

where σ is the shape factor, k is the permeability, μ is the viscosity, p_m is the matrix pressure, and p_f is the fracture pressure.

3.5.1. Mass transfer between natural fractures and inorganic pore network

Between natural fractures and inorganic pore networks, the inorganic pore networks have lower flow capacity. The mass transfer rate between them is controlled by gas flow in inorganic pores networks. In this case, flow mechanism of mass transfer is Slip flow. The difference between Slip flow and Darcy flow is in the apparent permeability, so the above mass transfer equation (Eq. (18)) can be applied to this situation with change on apparent permeability only:

$$Q_{f-na} = \sigma_{na} \frac{k_{slip}}{\mu} \rho \left(p_{na} - p_f \right) = \sigma_{na} F \frac{k_{na}}{\mu} \rho \left(p_{na} - p_f \right) \tag{19}$$

$$\sigma_{na} = \frac{12}{L_m^2} \tag{20}$$

where L_m is spacing of natural fractures and σ_{na} is the shape factor of inorganic pore networks.

Please cite this article in press as: Peng, Y., et al., A sequential model of shale gas transport under the influence of fully coupled multiple processes, Journal of Natural Gas Science and Engineering (2015), http://dx.doi.org/10.1016/j.jngse.2015.09.031

3.5.2. Mass transfer between inorganic pores networks and kerogen

Compared with inorganic pore networks, kerogen has the lower flow capacity. It means that the mass transfer rate between inorganic pore networks and kerogen is controlled by diffusion. The driving force of diffusion is the gas concentration difference. In this case, the molar transfer rate depends on the concentration difference between these two pore systems:

$$Q_{con} = \sigma_{ke} D_k \phi_{ke} (C_{ke} - C_{na}) \tag{21}$$

where D_k is the diffusivity. For the free gas, the concentration of gas has a linear relationship with its density. Multiplying the molar mass, the above equation of molar transfer rate can be converted to the mass transfer rate:

$$Q_{na-ke} = Q_{con} M = \sigma_{ke} D_k \phi_{ke} (\rho_{ke} - \rho_{na}) \tag{22}$$

$$\sigma_{ke} = \frac{12}{L_{ke}^2} \tag{23}$$

where L_{ke} is the spacing of inorganic pores, M is the molar mass and σ_{ke} is the shape factor of kerogen.

3.6. Final formulation of governing equation

According to the ideal gas law, the gas density is:

$$\rho = \frac{M}{RT} p \tag{24}$$

where M is molecular mass, T is temperature and R is universal constant. Substituting Eqs. (19), (22) and (24) into Eqs. (8), (13) and (17), final governing equations of gas flow in shales are:

(a) Gas Flow in Natural Fractures:

$$\phi_f \frac{\partial p_f}{\partial t} + \nabla\left(-\frac{k_f}{\mu} p_f \nabla p_f \right) = \sigma_{na} F \frac{k_{na}}{\mu} p_{na} \left(p_{na} - p_f \right) \tag{25}$$

(b) Gas Flow in Inorganic pores Networks:

$$\phi_{na} \frac{\partial p_{na}}{\partial t} + \nabla\left(-F \frac{k_{na}}{\mu} p_{na} \nabla p_{na} \right) = \sigma_{na} F \frac{k_{na}}{\mu} p_{na} \left(p_f - p_{na} \right) + \sigma_{ke} \phi_{ke} D_k (p_{ke} - p_{na}) \tag{26}$$

(c) Gas Flow in kerogen:

$$\left(\phi_{ke} + p_{ga} \rho_s \frac{V_L P_L}{(P_L + p_{ke})^2} \right) \frac{\partial p_{ke}}{\partial t} = \sigma_{ke} D_k \phi_{ke} (p_{na} - p_{ke}) \tag{27}$$

(d) Deformation of shales:

$$G u_{i,kk} + \frac{G}{1-2v} u_{k,ki} - \alpha_f p_{f,i} - \alpha_{na} p_{na,i} - \alpha_{ke} p_{ke,i} - \varepsilon_{s,i}(p_{ke}) + f_i = 0 \tag{28}$$

3.7. Intrinsic permeability model

As discussed earlier, apertures of natural fractures and inorganic pores are varying with pressure depletion of shale reservoir. Since shale is a multi-porosity medium, our previous concept of global and local strain (Peng et al., 2014b) for dual-porosity medium is introduced and further developed into this study.

The intrinsic permeability can be described as function of effective strain (Liu et al., 2011):

$$\frac{k}{k_0} = \left(\frac{\phi}{\phi_0} \right)^3 = \left(1 + \frac{1}{\phi_0} \Delta\varepsilon_e \right)^3 \tag{29}$$

For natural fractures, the effective strain is (Peng et al., 2014b):

$$\Delta\varepsilon_{fe} = \Delta\varepsilon_v - \Delta\varepsilon_{fl} = \Delta\varepsilon_v + \frac{\Delta p_f - \alpha_{na}\Delta p_{na} - \alpha_{ke}\Delta p_{ke}}{K_{na}} - \Delta\varepsilon_s(p_{ke}) \tag{30}$$

where ε_v is the volumetric strain, ε_{fl} is the local strain of natural fractures which contain two items. The first item represents the compressive strain of matrix containing inorganic pores. The second item represents the adsorbed-strain in kerogen. The local strain represents interactions between microscopic systems in shales. K_{na} is the bulk modulus of inorganic matrix part.

For inorganic pores, the effective strain is (Peng et al., 2014b):

$$\Delta\varepsilon_{nae} = \Delta\varepsilon_v - \frac{\Delta p_f - \alpha_{na}\Delta p_{na} - \alpha_{ke}\Delta p_{ke}}{K_{na}} + \frac{\Delta p_{na} - \alpha_{ke}\Delta p_{ke}}{K_{ke}} \tag{31}$$

where K_{ke} is the bulk modulus of kerogen. The last two terms represent interactions between microscopic structures in shales. Substituting Eq. (30) into Eq. (29), the porosity and intrinsic permeability models for natural fractures can be obtained:

$$\frac{\phi_f}{\phi_{f0}} = \left(1 + \frac{1}{\phi_{f0}} \left(\Delta\varepsilon_v + \frac{\Delta p_f - \alpha_{na}\Delta p_{na} - \alpha_{ke}\Delta p_{ke}}{K_{na}} - \Delta\varepsilon_s(p_{ke}) \right) \right) \tag{32}$$

$$\frac{k_f}{k_{f0}} = \left(1 + \frac{1}{\phi_{f0}} \left(\Delta\varepsilon_v + \frac{\Delta p_f - \alpha_{na}\Delta p_{na} - \alpha_{ke}\Delta p_{ke}}{K_{na}} - \Delta\varepsilon_s(p_{ke}) \right) \right)^3 \tag{33}$$

Substituting Eq. (31) into Eq. (29), the porosity and intrinsic permeability models for inorganic pores are:

$$\frac{\phi_{na}}{\phi_{na0}} = \left(1 + \frac{1}{\phi_{na0}} \left(\Delta\varepsilon_v - \frac{\Delta p_f - \alpha_{na}\Delta p_{na} - \alpha_{ke}\Delta p_{ke}}{K_{na}} + \frac{\Delta p_{na} - \alpha_{ke}\Delta p_{ke}}{K_{ke}} \right) \right) \tag{34}$$

$$\frac{k_{na}}{k_{na0}} = \left(1 + \frac{1}{\phi_{na0}} \left(\Delta\varepsilon_v - \frac{\Delta p_f - \alpha_{na}\Delta p_{na} - \alpha_{ke}\Delta p_{ke}}{K_{na}} + \frac{\Delta p_{na} - \alpha_{ke}\Delta p_{ke}}{K_{ke}} \right) \right)^3 \tag{35}$$

4. Model verification against experimental observations

Recently, experimental work on the evolution of shale permeability with effective stress has been widely reported (e.g. Ghanizadeh et al., 2015; Heller et al., 2014; Tinni et al., 2012). Plug samples containing fractures were used in these experiments. It was believed that the measured permeability from these samples is the fracture permeability in our model. In laboratory, the matrix permeability can be measured using crushed samples. However, crushed samples may also contain micro-fractures (Ghanizadeh

Please cite this article in press as: Peng, Y., et al., A sequential model of shale gas transport under the influence of fully coupled multiple processes, Journal of Natural Gas Science and Engineering (2015), http://dx.doi.org/10.1016/j.jngse.2015.09.031

et al., 2015; Tinni et al., 2012). Therefore, the true matrix permeability data were not valid in these researches. In addition, the effective stress is difficult, if not impossible, to be applied on crushed samples. . Therefore, these experimental data only allow verifying the intrinsic natural fracture permeability model.

In the experiments, the boundary condition of plug samples is confining pressure (σ_{con}) which is simplified as shown Fig. 5 (a). Because of the symmetry, the 3-D shale sample shown in Fig. 5 (a) could be represented by the 2-D model shown in Fig. 5 (b). The relationship of 2-D model geometry with 3-D geometry is illustrated as the red plane in Fig. 5 (a). In addition, the porosity of natural fracture is less than 0.5% (Wang and Reed, 2009). Young's modulus decreases with content of clay + kerogen and it has a wide range from 5.5 to 86 GPa (Sone and Zoback, 2013). The input parameters for verifying the model are listed in Tables 1 and 2.

The comparison between experimental data and simulation data is shown as Fig. 6. The lines are model results. It is obvious that the model can represent the experimental data very well. Other models of intrinsic permeability for shales have been proposed by fitting experimental data (e.g. Kwon et al., 2001; Dong et al., 2010; Petunin et al., 2011; Tinni et al., 2012). Compared with those models, this model has a clearer physical meaning: the intrinsic permeability is a result of the difference between volumetric strain of shale sediments and local strain of pores. Moreover, this model is derived from poroelastic theory so it can be applied to any mechanical boundary conditions.

5. Investigation of effect of pore structure on shale gas production

In order to investigate effects of pore structure on shale gas production, a simulation model was constructed as shown in Fig. 7(b). Due to the symmetry of hydraulic fracture networks, a quarter of the overall area between two hydraulic fractures, illustrated as the red rectangle in Fig. 7(a), was selected. The height of the reservoir model is half length of hydraulic fractures, and the width is the half hydraulic fractures spacing. The mechanical condition of shale deformation is uniaxial strain. The overburden stress is applied at the top boundary and kept constant. The boundary conditions of gas flow are: (1) for natural fractures and inorganic pore networks, the pressure, which represents the pressure in hydraulic fractures, is applied at the right boundary; no flow condition

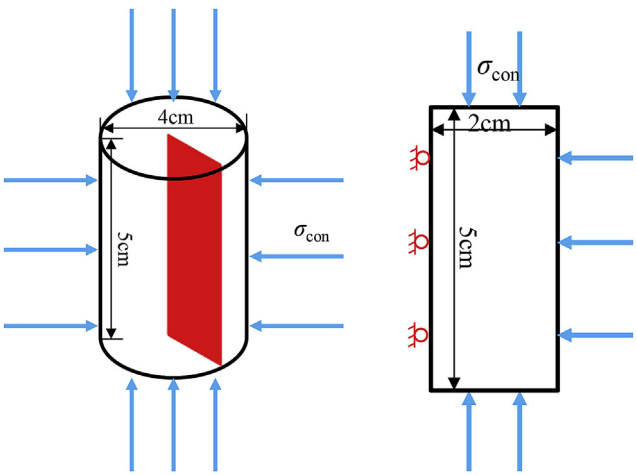

Fig. 5. Illustration of Geometry in numerical simulations.

Table 1
Input parameters for verifying simulations for experiments conducted by Ghanizadeh et al.

Sample	ϕ_0 (%)	E (GPa)	ν (−)	ρ_c (kg/m^3)
1	0.2	60	0.2	2500
2	0.15	60	0.2	2500
3	0.1	60	0.2	2500

Table 2
Input parameters for verifying simulations for experiments conducted by Heller et al.

Pore pressure (psi)	ϕ_0 (%)	E (GPa)	ν (−)	ρ_c (kg/m^3)
250	0.3	55	0.3	2500
500	0.28	55	0.3	2500
1000	0.26	55	0.3	2500
2000	0.25	55	0.3	2500
3000	0.25	55	0.3	2500
4000	0.25	55	0.3	2500

is applied at other boundaries; (2) For the kerogen, no flow condition is applied at all boundaries because gas in kerogen is assumed to only flow into other two pore systems (natural fractures and inorganic pores networks). The initial pressure is P_0. Input parameters for shales are listed in Table 3. They were collected from literatures (Chen et al., 2015; Pan and Connell, 2015; Sone and Zoback, 2013; Wang and Reed, 2009). In this study, a time-dependent pressure was applied to the hydraulic fracture to simulate the pressure change during production:

$$p_{hy} = P_0 - \Delta p\left(1 - e^{-t/td}\right) \tag{36}$$

where p_{hy} is pressure in the hydraulic fracture, t is time, P_0 is the initial pressure of reservoir, Δp is the pressure drop between initial pressure and the final pressure of reservoir, t_d is the characteristic time to control pressure drop. It is noted that this pressure behaviour, described in Eq. (36) and plotted in Fig. 8, is only hypothetical and in reality, the pressure in the fracture is impacted by the reservoir flow behaviour as well as the well operating conditions. Nevertheless, since this is sensitivity analysis of gas production to the key reservoir parameters, using this hydraulic fracture pressure curve is appropriate as it is kept the same for all the simulation cases.

5.1. Gas flow sequence

Evolutions of pressures in natural fracture, inorganic pores and organic pores at the point 0.2 m away from hydraulic fracture are shown in Fig. 9. Initially, pressures in all three pore systems are all equal to the initial pressure. When the production commences, they start to decline. Due to the difference in flow capacity for different pore systems, the pressures decline with different magnitudes. Gas in natural fracture is easy to flows into hydraulic fractures and its pressure declines most quickly. Compared with natural fractures, the inorganic pores network has a lower flow capacity, so the evolution of its pressure lags behind that in natural fractures. Among these three flow regimes, the diffusion is most difficult to occur so its pressure is the highest during the production. After 100 days, the pressure in the inorganic pore network is a slightly higher than the pressure in natural fracture. It is mainly resulted from the permeability variation. During the gas production, natural fracture permeability decreases. When it decreases to a the extent that the flow capacity of natural fracture is less than that of inorganic pore network, the gas flow in inorganic pore

Please cite this article in press as: Peng, Y., et al., A sequential model of shale gas transport under the influence of fully coupled multiple processes, Journal of Natural Gas Science and Engineering (2015), http://dx.doi.org/10.1016/j.jngse.2015.09.031

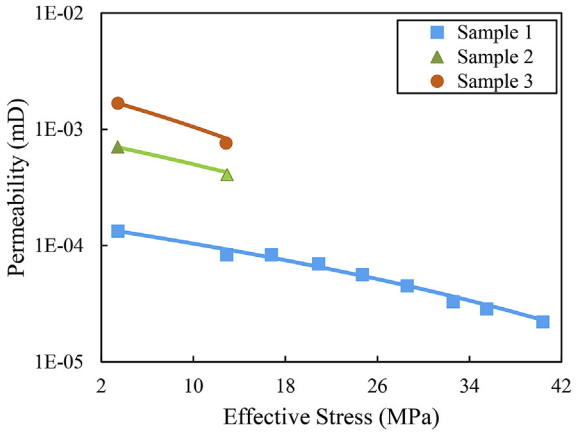

(a) Permeability Evolution with Effective Stress obtained by Ghanizadeh et al. (2015) (lines are simulation results).

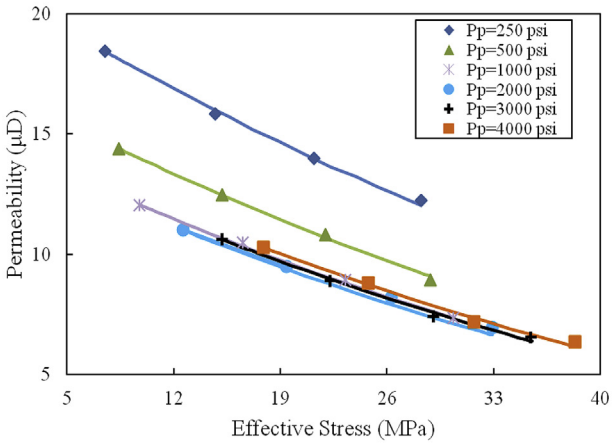

(b) Permeability Evolution with Effective Stress obtained by Heller et al. (2014) (lines are simulation results).

Fig. 6. Comparison between experimental data and simulation data.

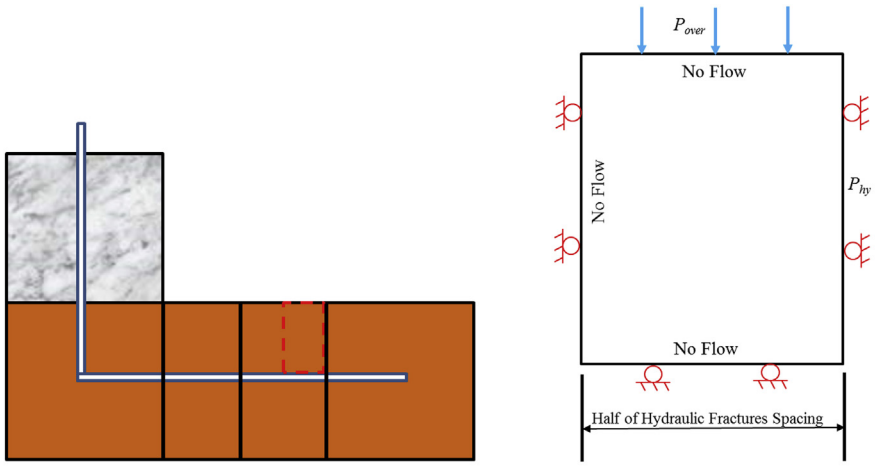

(a) Illustration of Shale Reservoir (b) Geometry of Numerical Simulation Model

Fig. 7. Simulation model of shale gas flow into hydraulic fractures.

network would be a production rate dominating factor. In this case, the pressure drop in inorganic pore network would exceed that in the natural fractures.

Fig. 9 also presents the sequential flow process in shale gas flow. This process is consistent with experimental observation by Javadpour et al. (2007): Flows in natural fractures and inorganic pores occur first (stage A and B in Fig. 2). The flow in natural fracture networks is the faster one and it dominates gas flow in the

Please cite this article in press as: Peng, Y., et al., A sequential model of shale gas transport under the influence of fully coupled multiple processes, Journal of Natural Gas Science and Engineering (2015), http://dx.doi.org/10.1016/j.jngse.2015.09.031

Table 3
Input parameters.

Symbol	Value	Physical meanings	Unit
E	20	Young's modulus of Shale	GPa
ν	0.3	Poisson's ratio of Shale	–
μ	1.3×10^{-5}	Viscosity	Pa s
ϕ_{na0}	4	Initial inorganic pores porosity	%
ϕ_{f0}	0.1	Initial natural fracture porosity	%
ϕ_{ke0}	1	Initial natural kerogen porosity	%
k_{na0}	1×10^{-21}	Initial inorganic pores permeability	m^2
k_{f0}	1×10^{-19}	Initial natural fracture permeability	m^2
r_{na}	20	Radius of inorganic pores	nm
α	0.5	tangential momentum accommodation coefficient	–
L_m	1	Spacing of natural fractures	m
L_{ke}	0.5	Spacing of matrix blocks	m
D_k	1×10^{-10}	Diffusivity in kerogen	m/s
M	0.016	Molecular mass	kg/mol
R	8.314	Universal gas constant	J/mol/K
T	350	Temperature	K
P_0	40	Initial pressure	MPa
P_L	10	Langmuir pressure constant of Methane	MPa
P_{over}	40	Overburden pressure	MPa
ε_L	0.0005	Langmuir strain constant of Methane	–
ρ_s	2500	Shale density	kg/m^3
P_a	0.1	Atmosphere pressure	MPa
α_f	0.67	Biot coefficient of shales	–
α_{na}	0.67	Biot coefficient of matrix blocks with inorganic pores	–
α_{ke}	0.67	Biot coefficient of kerogen	–
η	50	Thickness of reservoir	m
λ	30	Number of stimulated stages by hydraulic fracking in whole reservoir	–
V_L	0.002	Langmuir volume constant of Methane	m^3/kg
Δp	35	Pressure drop of reservoir	MPa
t_d	1.25×10^6	Characteristic time of pressure drop	1/s

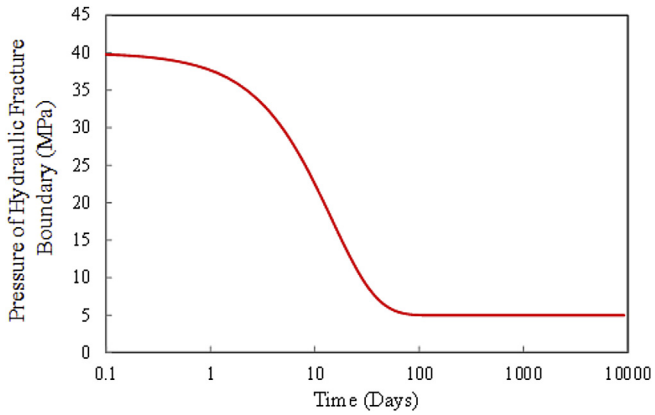

Fig. 8. Curve of pressure at hydraulic fracture boundary.

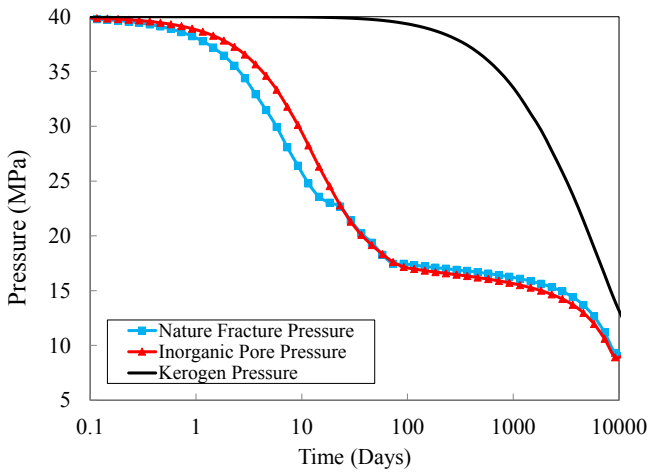

Fig. 9. Evolution of pressure with time.

early stage of production. Following that, gas flow in inorganic pores dominates production; the diffusion and desorption (stage C and D in Fig. 2) occur the latest. Due to this sequential flow process, a wide variation in pressure between different pore systems is created as shown in Fig. 9. In this case, using only one single pressure to calculate permeability evolution is improper because, single-porosity model (only one pressure can be solved) cannot describe the different pressures in different pore systems.

5.2. Permeability evolutions

Permeability has a close relationship with pressures in shales. Fig. 10 shows the evolution of natural fracture permeability with natural fracture pressure. With depletion of gas, the natural fracture permeability declines sharply. Fig. 11 illustrates the evolution of the apparent permeability of inorganic pore system, its intrinsic permeability and correlation coefficient. During the gas depletion, intrinsic permeability of inorganic pores declines like natural fracture permeability and then increase slightly at lower pressure. From Fig. 9, when inorganic pores pressure reaches around 15 MPa, the pressure in organic pores of the kerogen starts to decrease. It triggers interactions between organic pores and inorganic pores, leading to increase of the intrinsic permeability. Correlation coefficient is mainly controlled by shale gas state and it increases with gas pressure decline. The apparent permeability is the resultant of these two (Eq. (1)). For parameters of this study, the intrinsic permeability dominates the apparent permeability.

The effect of deformation on inorganic pore permeability has not been introduced into simulations. For some simulations (e.g. Akkutlu and Fathi, 2012; Ding et al., 2014; Javadpour et al., 2007),

Please cite this article in press as: Peng, Y., et al., A sequential model of shale gas transport under the influence of fully coupled multiple processes, Journal of Natural Gas Science and Engineering (2015), http://dx.doi.org/10.1016/j.jngse.2015.09.031

the apparent permeability of inorganic pores is controlled only by correlation coefficient. They suggested that the apparent permeability of inorganic pores increases during gas production. From Fig. 11, it can be clearly seen that the large error would occur by this assumption at the similar condition as in this study. If the geomechanical effect was considered, the apparent permeability could decrease instead of increase. For other simulations (e.g. Civan et al., 2011), the effect of geomechanical deformation on intrinsic permeability was introduced while effects of boundary condition on intrinsic permeability were ignored. Boundary conditions of rocks strongly affect effective stress so these models cannot be used for both experiments and fields where boundary conditions are different. In addition, these experiments only considered one flow regime in shales so these models (e.g. Raghavan and Chin, 2002; Dong et al., 2010) relate to only one kind of pore pressure. It fails to consider the effect of coexistence of several flow regimes on intrinsic permeability. The model developed in this paper used the relationship of intrinsic permeability with effective strain. The effective strain for different boundary conditions can be calculated by the equation of motion for the shale (Eq. (3)). The intrinsic permeability model is therefore valid under any boundary condition. Furthermore, the permeability models in this paper consider effects of mass transfer between different pore systems as well as adsorption-induced strain.

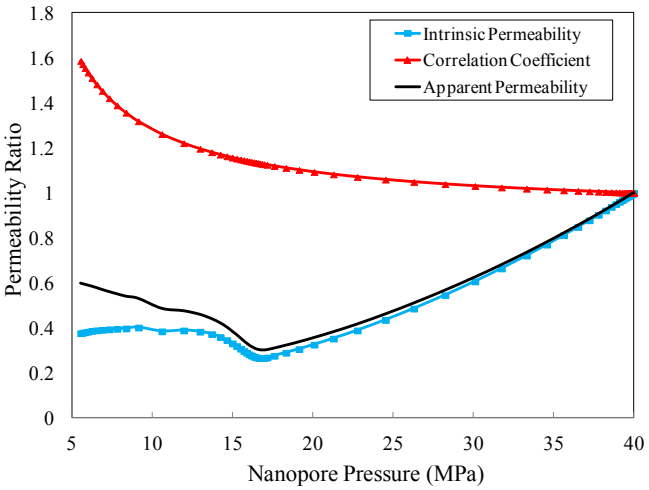

Fig. 11. Evolution of permeability ratios of inorganic pores with inorganic pores pressure.

5.3. Effect of deformation

The effect of deformation on shale gas production is often ignored and therefore the characteristic of permeability variation from the shale deformation cannot be described for shale gas production. In this section, the importance of deformation effect on shale gas production is investigated. To achieve it, comparison between two simulations was conducted: one is fully coupled simulation and the other one ignores the deformation of shale. All parameters in the two simulation cases are the same as shown in Table 3. In the simulation without deformation, intrinsic permeabilities for natural fractures and inorganic pores networks are kept constant during gas production. For the fully coupled simulation, intrinsic permeabilities change similarly to that shown in Figs. 10 and 11.

In this paper, the gas in inorganic pore networks and natural fractures were both allowed to flow into hydraulic fractures. The production rate is the summation of these two flow rates. Fig. 12 (a) shows the evolutions of total production rate, rate contributed by gas flow from natural fracture and that contributed by gas flow from inorganic pores. Fig. 12 (b) shows the rates for a case without reservoir deformation. In the fully coupled simulation, the gas flow from natural fractures dominates the production rate before 20 days. After that, the gas flow from inorganic pores networks dominates. Compared to the case with reservoir deformation, the gas flow from natural fractures always dominates the shale gas production rate for the case without reservoir deformation. The gas flow rate from inorganic pore network is two orders of magnitude lower than that from natural fracture. Even if the porosity of natural fracture is only one fortieth of porosity of the inorganic pore networks, it still provides an efficient flow path for gas due to its large pore size and high permeability. However, if reservoir deformation was considered, natural fractures were narrowed during gas depletion. When it declines to the extent that makes its flow capacity less than that of inorganic pore network, the gas flow in inorganic pore networks starts to be the main flow path for shale gas production.

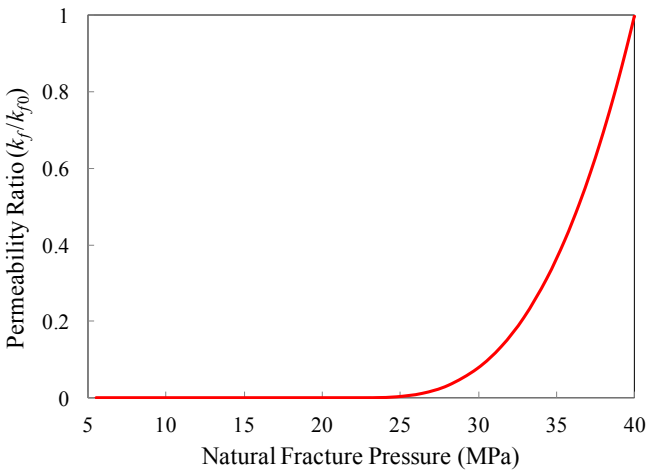

Fig. 10. Evolution of permeability ratio of natural fracture with natural fracture pressure.

Because of this huge difference in production rate between these two scenarios, the recovery efficiencies of shale gas for these two scenarios are also different. The recovery efficiency is the ratio of the amount of produced shale gas to the initial gas in place. As shown in Fig. 13, if the deformation effect was not considered, the recovery efficiency is predicted at 75% after 30 years of production while it is only 29% when the deformation effect was considered. This huge difference is resulted from the difference in apparent permeability change in the different pore systems. From this comparison, it is apparent that the deformation would significantly affect shale gas production behaviour.

5.4. Importance of natural fracture

Although the flow in natural fracture near the hydraulic fracture only affects production at early production stage, the flow in natural fracture inside reservoir plays an important role in the long term gas transport. Fig. 14 illustrates the gas velocity at a point 6 m away from the hydraulic fracture. The gas velocity in the natural fracture is two orders of magnitudes higher than that in inorganic pores. It demonstrates that the natural fracture is the main flow path for shale gas far away from hydraulic fractures and it can enhance efficiency of gas transport from inside reservoir to hydraulic fracture. In addition, Fig. 15 shows the evolutions of

Please cite this article in press as: Peng, Y., et al., A sequential model of shale gas transport under the influence of fully coupled multiple processes, Journal of Natural Gas Science and Engineering (2015), http://dx.doi.org/10.1016/j.jngse.2015.09.031

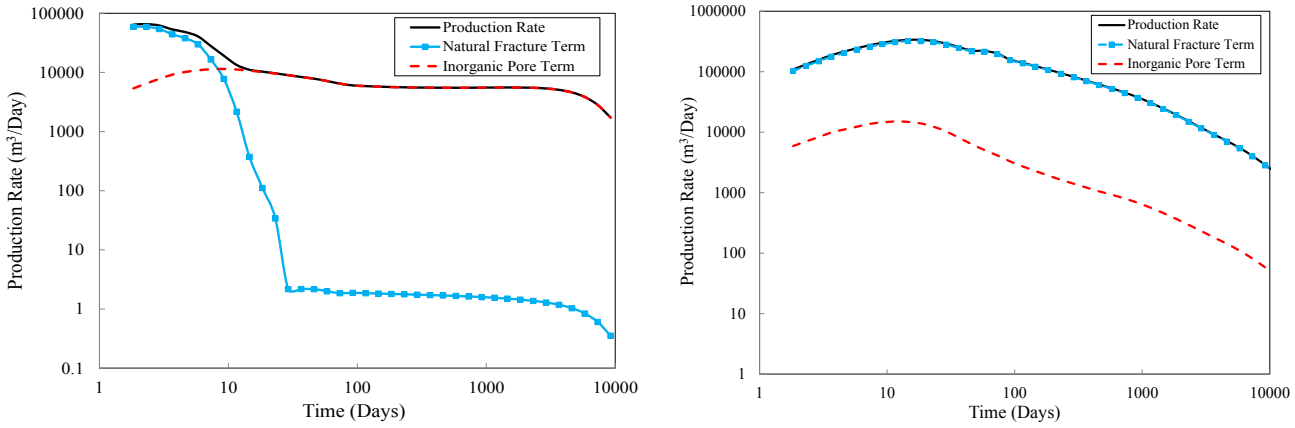

(a) Fully Coupled Simulation

(b) Simulation without Deformation

Fig. 12. Illustration of effects of deformation on shale gas production rate.

recovery efficiencies for the two scenarios: one considers the gas flow in natural fractures and the other does not. The recovery efficiency for the scenario with flow in natural fracture is 29% while that for the other scenario is only 12.3%. The flow in natural fracture enhances the recovery efficiency over 2 times. Although natural fracture only accounts for small proportion of flow path in reservoirs (its porosity is only 0.1% which is one-fortieth of porosity of inorganic pores), it plays a much more important role in gas transport inside reservoirs and enhancement of shale gas production.

5.5. Sensitivity analysis

In this model, many parameters strongly affect shale gas production. The analysis of their effects on shale gas production is valuable for production designs and managements. In this section, effects of natural fracture permeability (k_f), natural fracture porosity (ϕ_f), intrinsic permeability of inorganic pores (k_{na}), Young's modulus of shales (E) and the ratio of adsorbed gas to total gas (β) were investigated. The definition of β is:

$$\beta = \frac{m_{ad}}{m_t} = \frac{V\rho_{ad}}{V\rho_t} = \frac{\frac{p_a\rho_c V_L}{P_L+P_0}}{\phi_f + \phi_{na} + \phi_{ke} + \frac{p_a\rho_c V_L}{P_L+P_0}} \tag{37}$$

where m_{ad} is the mass of adsorbed gas at the initial condition, m_t is

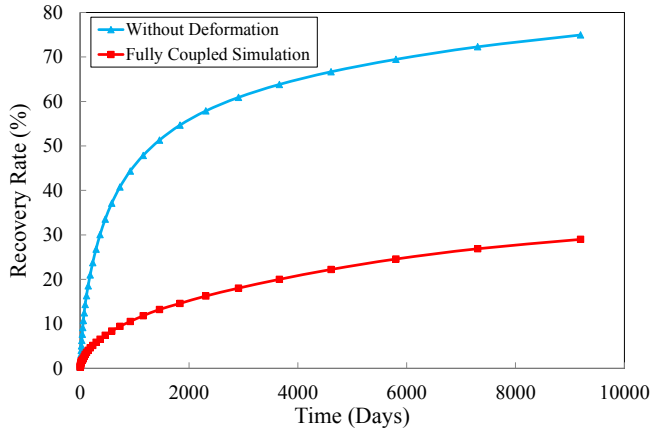

Fig. 13. Illustration of effects of deformation on shale gas recovery rate.

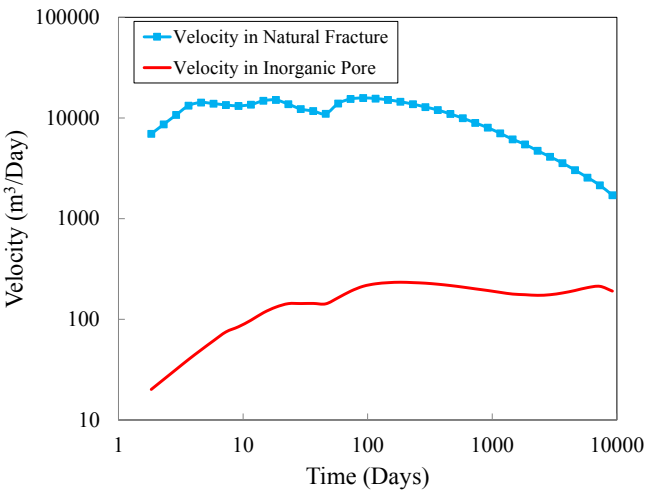

Fig. 14. Illustration of Importance of Flow in Natural Fracture on Recovery Rate (The coordinate of the Point is (24, 25)).

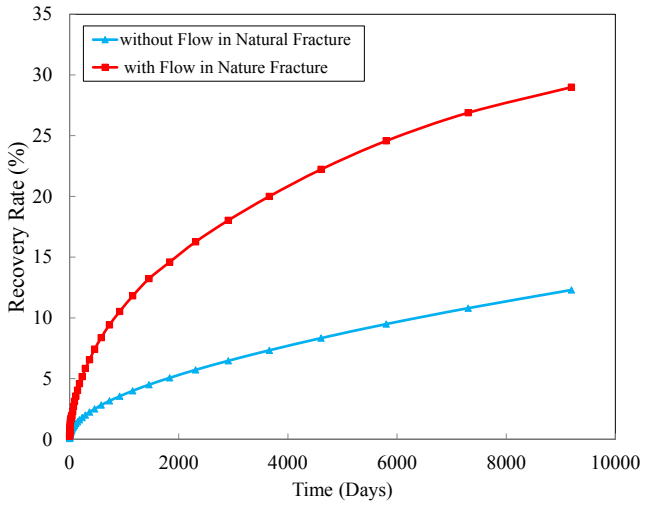

Fig. 15. Illustration of importance of flow in natural fracture on recovery rate.

Please cite this article in press as: Peng, Y., et al., A sequential model of shale gas transport under the influence of fully coupled multiple processes, Journal of Natural Gas Science and Engineering (2015), http://dx.doi.org/10.1016/j.jngse.2015.09.031

Table 4
Values of V_L and β

V_L (m^3/kg)	β (%)
0.002	16
0.004	28
0.01	50

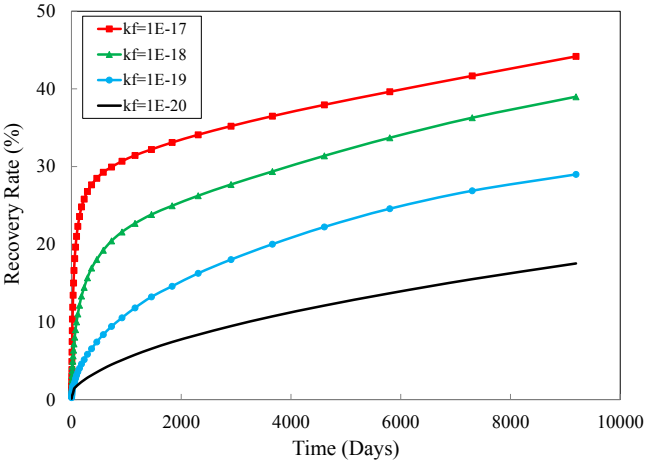

Fig. 16. Illustration of Effect of k_f on Recovery Rate.

the total mass of gas in reservoirs at the initial condition, V is the reservoir volume, ρ_{ad} is the density of adsorbed gas in reservoirs, ρ_t is the total density of gas in reservoirs and it contains free-phase gas in kerogen, inorganic pores and natural fractures, and adsorbed gas. For simplification, all parameters, except V_L, are constant. In this case, the value of β is controlled by V_L. The value of V_L and its corresponding value of β are listed in Table 4. For the base case, parameters in Table 3 were used. In the parameter sensitivity analyses, only one parameter is changed at a time while the rest were kept constant values same as the base case. Fig. 16 shows the effect of k_f on recovery efficiency. If the k_f increases 1000 times, the recovery efficiency increases 2.5 times. Since natural fracture dominates gas transport inside reservoirs, higher k_f means higher flow capacity to gas transport towards hydraulic fractures. Fig. 17 shows the effect of ϕ_f on recovery efficiency. If the ϕ_f increases 5 times, the

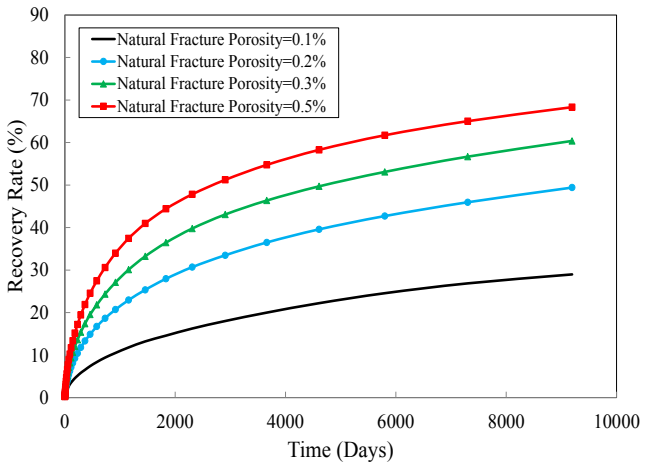

Fig. 17. Illustration of Effect of ϕ_f on Recovery Rate.

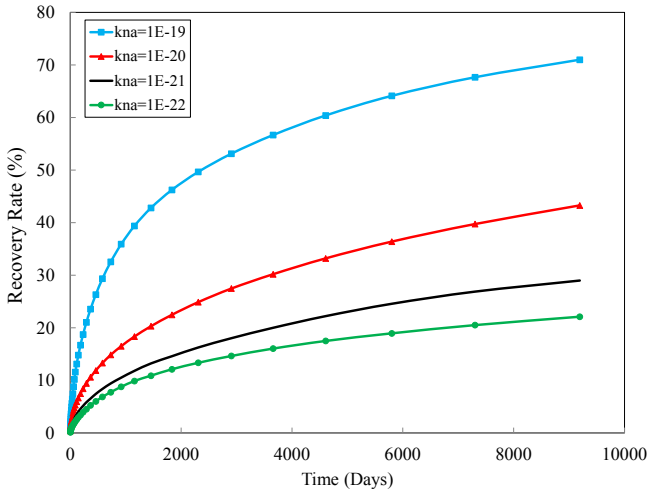

Fig. 18. Illustration of Effect of k_{na} on Recovery Rate.

recovery efficiency increases 2.4 times. The recovery efficiency increases with ϕ_f because the higher ϕ_f also provides more flow paths to shale gas production. Fig. 18 illustrates effect of k_{na} on recovery efficiency. If the k_{na} increases 1000 times, the recovery efficiency increases 3.2 times. For parameters used in this study, the inorganic pores network dominates the production rate so higher k_{na} also means higher flow capacity to shale gas production. Fig. 19 presents effect of E on recovery rate. If the E increases 2.7 times, the recovery efficiency increases 2.4 times. Young's Modulus represents the geomechanical effect on shale gas production. The higher E means that the shale is stiffer to deform so negative impact of deformation on permeability variation reduces during gas depletion. In this case, both the gas transport inside reservoirs and production rate will be enhanced so the recovery efficiency increases with E. Fig. 20 shows effect of the ratio of adsorbed gas (β) on recovery efficiency. It has a negative linear relationship with recovery efficiency: increase of β leads to the decrease of recovery efficiency. The adsorbed gas is the most difficult proportion to be produced due to its low flow capacity. Its negative relationship with recovery efficiency means that the more adsorbed gas in reservoir, the less amount of gas can be released from reservoir.

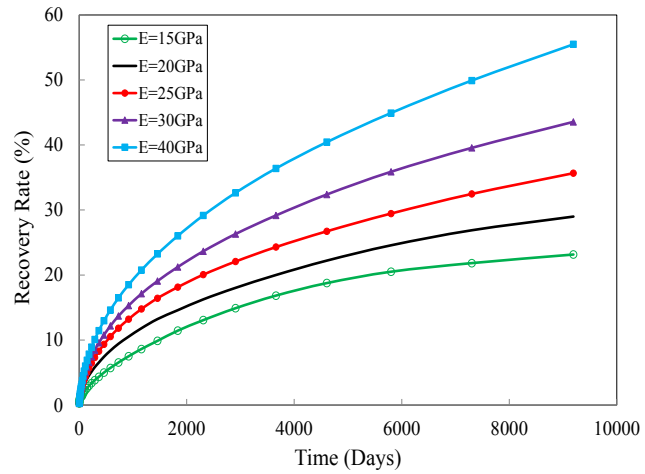

Fig. 19. Illustration of effect of E on recovery rate.

Please cite this article in press as: Peng, Y., et al., A sequential model of shale gas transport under the influence of fully coupled multiple processes, Journal of Natural Gas Science and Engineering (2015), http://dx.doi.org/10.1016/j.jngse.2015.09.031

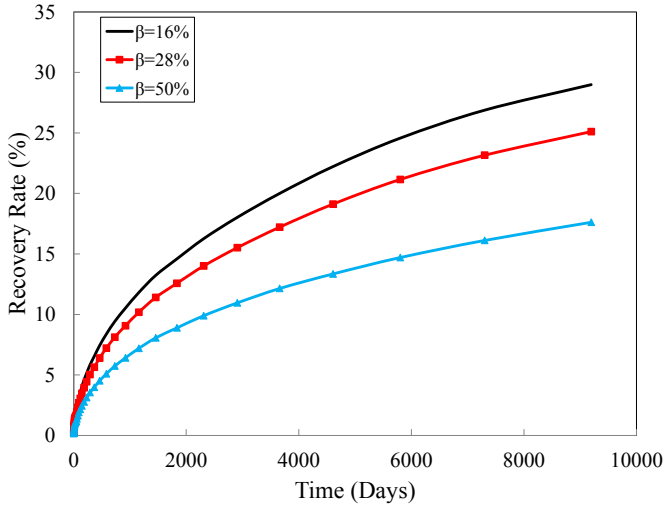

Fig. 20. Illustration of Effect of β on Recovery Rate.

6. Conclusion

In this study, deformation effect on permeability variation was introduced into a multi-scale numerical simulation model for shale gas transport. The main advantages of the proposed model are: (1) models of intrinsic permeability were built based on poroelastic theory, allowing these models to be validly used under any boundary condition; (2) interactions between different pore systems were considered to represent different behaviour of permeability changes for different pore systems in shales. Using this numerical simulation model, important factors in shale gas production were analysed and the following main conclusions were drawn:

(1) Deformation effect plays an important role in the apparent permeability. Without deformation effect, the apparent permeability increases during shale reservoir depletion. Deformation can significantly reduce the magnitude of apparent permeability increase or even make apparent permeability decrease. It suggests that analysis conducted by models without deformation effect would overestimate shale gas production rate. In addition, because of interactions between different pore systems, apparent permeability of different pore systems behaves differently.
(2) Natural fracture plays significant role in gas transport in the reservoir. Unlike the place near hydraulic fracture, the gas velocity in natural fracture is much higher than that in inorganic pores. It enhances the efficiency of gas transport from reservoir to hydraulic fracture. It suggests that gas flow in natural fracture should not be ignored in analysing shale gas production and keeping natural fracture open and creation of natural fractures are important for shale gas production.
(3) Natural fracture permeability, natural fracture porosity, inorganic pores permeability and Young's modulus have a positive relation with gas production. However, the percentage of adsorbed gas to total gas (β) has a negative relation with recovery rate of gas.

Acknowledgements

This work is partially funded by National Natural Science Foundation of China (51474204). This support is gratefully acknowledged.

References

Akkutlu, I.Y., Fathi, E., 2012. Multiscale gas transport in shales with local Kerogen heterogeneities. SPE J. 17, 1,002–001,011.
Bear, J., Bachmat, Y., 1990. Introduction to Modeling of Transport Phenomena in Porous Media, vol. 4. Springer Science & Business Media.
Carlson, E.S., Mercer, J.C., 1991. Devonian shale gas production: mechanisms and simple models. J. Pet. Technol. 43 (04), 476–482.
Chen, T., Feng, X.-T., Pan, Z., 2015. Experimental study of swelling of organic rich shale in methane. Int. J. Coal Geol. 150–151, 64–73.
Cho, Y., Ozkan, E., Apaydin, O.G., 2013. Pressure-dependent natural-fracture permeability in shale and its effect on shale-gas well production. SPE Reserv. Eval. Eng. 16, 216–228.
Civan, F., Rai, C.S., Sondergeld, C.H., 2011. Shale-gas permeability and diffusivity inferred by improved formulation of relevant retention and transport mechanisms. Transp. Porous Media 86, 925–944.
Curtis, J.B., 2002. Fractured shale-gas systems. AAPG Bull. 86, 1921–1938.
Ding, D.Y., Wu, Y.-S., Farah, N., Wang, C., Bourbiaux, B., 2014. Numerical Simulation of Low Permeability Unconventional Gas Reservoirs.
Dong, J.-J., Hsu, J.-Y., Wu, W.-J., Shimamoto, T., Hung, J.-H., Yeh, E.-C., Wu, Y.-H., Sone, H., 2010. Stress-dependence of the permeability and porosity of sandstone and shale from TCDP Hole-A. Int. J. Rock Mech. Min. Sci. 47, 1141–1157.
Gale, J.F., Reed, R.M., Holder, J., 2007. Natural fractures in the Barnett shale and their importance for hydraulic fracture treatments. AAPG Bull. 91, 603–622.
Ghanizadeh, A., Bhowmik, S., Haeri-Ardakani, O., Sanei, H., Clarkson, C.R., 2015. A comparison of shale permeability coefficients derived using multiple non-steady-state measurement techniques: examples from the Duvernay Formation, Alberta (Canada). Fuel 140, 371–387.
Gray, I., 1987. Reservoir engineering in coal seams: part 1-The physical process of gas storage and movement in coal seams. SPE Reserv. Eng. 2, 28–34.
Guo, C., Xu, J., Wu, K., Wei, M., Liu, S., 2015. Study on gas flow through nano pores of shale gas reservoirs. Fuel 143, 107–117.
Han, F., Busch, A., Krooss, B.M., Liu, Z., van Wageningen, N., Yang, J., 2010. Experimental study on fluid transport processes in the cleat and matrix systems of coal. Energy Fuels 24, 6653–6661.
Harpalani, S., Chen, G., 1997. Influence of gas production induced volumetric strain on permeability of coal. Geotech. Geol. Eng. 15, 303–325.
Heller, R., Vermylen, J., Zoback, M., 2014. Experimental investigation of matrix permeability of gas shales. AAPG Bull. 98, 975–995.
Javadpour, F., 2009. Nanopores and apparent permeability of gas flow in mudrocks (Shales and siltstone). J. Can. Pet. Technol. 48, 16–21.
Javadpour, F., Fisher, D., Unsworth, M., 2007. Nanoscale gas flow in shale gas sediments. J. Can. Pet. Technol. 46, 55–61.
Kang, S.M., Fathi, E., Ambrose, R.J., Akkutlu, I.Y., Sigal, R.F., 2011. Carbon dioxide storage capacity of organic-rich shales. SPE J. 16, 842–855.
Kwon, O., Kronenberg, A.K., Gangi, A.F., Johnson, B., 2001. Permeability of Wilcox shale and its effective pressure law. J. Geophys. Res. Solid Earth 106, 19339–19353 (1978–2012).
Liu, H.-H., Rutqvist, J., 2010. A new coal-permeability model: internal swelling stress and fracture–matrix interaction. Transp. porous media 82 (1), 157–171.
Liu, J., Wang, J., Chen, Z., Wang, S., Elsworth, D., Jiang, Y., 2011. Impact of transition from local swelling to macro swelling on the evolution of coal permeability. Int. J. Coal Geol. 88 (1), 31–40.
Loucks, R.G., Reed, R.M., Ruppel, S.C., Hammes, U., 2012. Spectrum of pore types and networks in mudrocks and a descriptive classification for matrix-related mudrock pores. AAPG Bull. 96, 1071–1098.
Minkoff, S.E., Stone, C.M., Bryant, S., Peszynska, M., Wheeler, M.F., 2003. Coupled fluid flow and geomechanical deformation modeling. J. Pet. Sci. Eng. 38, 37–56.
Moghadam, A.A., Chalaturnyk, R., 2014. Expansion of the Klinkenberg's slippage equation to low permeability porous media. Int. J. Coal Geol. 123, 2–9.
Nelson, P.H., 2009. Pore-throat sizes in sandstones, tight sandstones, and shales. AAPG Bull. 93, 329–340.
Olsen, T., Brenize, G., Frenzel, T., 2003. Improvement processes for coalbed natural gas completion and stimulation. In: SPE Annual Technical Conference and Exhibition. Society of Petroleum Engineers.
Palmer, I., Mansoori, J., 1996. How permeability depends on stress and pore pressure in coalbeds: a new model. In: SPE Annual Technical Conference and Exhibition.
Palmer, I., Mavor, M., Gunter, B., 2007. Permeability Changes in Coal Seams During Production and Injection. Paper presented at the International Coalbed Methane Symposium. University of Alabama, Tuscaloosa, Alabama.
Pan, Z., Connell, L.D., 2015. Reservoir simulation of free and adsorbed gas production from shale. J. Nat. Gas Sci. Eng. 22, 359–370.
Peng, Y., Liu, J., Zhu, W., Pan, Z., Connell, L., 2014a. Benchmark assessment of coal permeability models on the accuracy of permeability prediction. Fuel 132, 194–203.
Peng, Y., Liu, J., Wei, M., Pan, Z., Connell, L., 2014b. Why coal permeability changes under free swellings: new insights. Int. J. Coal Geol. 133, 35–46.
Petunin, V.V., Yin, X., Tutuncu, A.N., 2011. Porosity and permeability changes in sandstones and carbonates under stress and their correlation to rock texture. In: Canadian Unconventional Resources Conference. Society of Petroleum Engineers.
Pruess, K., 1985. A practical method for modeling fluid and heat flow in fractured porous media. Soc. Pet. Eng. J. 25, 14–26.

Please cite this article in press as: Peng, Y., et al., A sequential model of shale gas transport under the influence of fully coupled multiple processes, Journal of Natural Gas Science and Engineering (2015), http://dx.doi.org/10.1016/j.jngse.2015.09.031

Raghavan, R., Chin, L., 2002. Productivity changes in reservoirs with stress-dependent permeability. In: SPE Annual Technical Conference and Exhibition. Society of Petroleum Engineers.
Ranjbar, E., Hassanzadeh, H., 2011. Matrix–fracture transfer shape factor for modeling flow of a compressible fluid in dual-porosity media. Adv. Water Resour. 34, 627–639.
Roy, S., Raju, R., Chuang, H.F., Cruden, B.A., Meyyappan, M., 2003. Modeling gas flow through microchannels and nanopores. J. Appl. Phys. 93, 4870–4879.
Rubin, B., 2010. Accurate simulation of non darcy flow in stimulated fractured shale reservoirs. In: SPE Western Regional Meeting. Society of Petroleum Engineers.
Rutqvist, J., Wu, Y.-S., Tsang, C.-F., Bodvarsson, G., 2002. A modeling approach for analysis of coupled multiphase fluid flow, heat transfer, and deformation in fractured porous rock. Int. J. Rock Mech. Min. Sci. 39, 429–442.
Shi, J.-Q., Durucan, S., 2005. A model for changes in coalbed permeability during primary and enhanced methane recovery. SPE Reserv. Eval. Eng. 8, 291–299.
Sondergeld, C.H., Ambrose, R.J., Rai, C.S., Moncrieff, J., 2010. Micro-structural studies of gas shales. In: SPE Unconventional Gas Conference. Society of Petroleum Engineers.
Sone, H., Zoback, M.D., 2013. Mechanical properties of shale-gas reservoir rocks—part 1: static and dynamic elastic properties and anisotropy. Geophysics 78, D381–D392.
Tinni, A., Fathi, E., Agarwal, R., Sondergeld, C., Akkutlu, Y., Rai, C., 2012. Shale Permeability Measurements on Plugs and Crushed Samples. SPE-162235.
Vera, F., Ehlig-Economides, C., 2013. Diagnosing pressure dependent permeability in long term shale gas pressure and production transient analysis. In: SPE Annual Technical Conference and Exhibition, New Orleans, Louisiana, USA. Society of Petroleum Engineers, p. 6000. SPE-166152-MS.
Wang, F.P., Reed, R.M., 2009. Pore networks and fluid flow in gas shales. In: SPE Annual Technical Conference and Exhibition. Society of Petroleum Engineers.
Wang, H., Xu, W., Zuo, J., 2014. Compact rock material gas permeability properties. Phys. B Condens. Matter 449, 10–18.
Warren, J., Root, P.J., 1963. The behavior of naturally fractured reservoirs. SPE J. 3 (3), 245–255.
Wu, Y., Liu, J., Elsworth, D., Chen, Z., Connell, L., Pan, Z., 2010. Dual poroelastic response of a coal seam to CO_2 injection. Int. J. Greenh. Gas Control 4, 668–678.
Ye, Z., Chen, D., Pan, Z., 2015. A unified method to evaluate shale gas flow behaviours in different flow regions. J. Nat. Gas Sci. Eng. 26, 205–215.
Zhang, H., Liu, J., Elsworth, D., 2008. How sorption-induced matrix deformation affects gas flow in coal seams: a new FE model. Int. J. Rock Mech. Min. Sci. 45, 1226–1236.

Please cite this article in press as: Peng, Y., et al., A sequential model of shale gas transport under the influence of fully coupled multiple processes, Journal of Natural Gas Science and Engineering (2015), http://dx.doi.org/10.1016/j.jngse.2015.09.031